CHAPTER 6

Dopants and Impurity-Induced Defects in ZnO

M. AZIZAR RAHMAN, MATTHEW R. PHILLIPS and CUONG TON-THAT*

School of Mathematical and Physical Sciences,
University of Technology Sydney, Ultimo, NSW 2007, Australia
*cuong.ton-that@uts.edu.au

In recent years, there has been resurgent interest in ZnO due to its efficient UV emission and potential application in opto-electronic devices. The problem of self-compensating defects, especially those related to acceptor-like dopants, remains a major challenge to date. In this chapter, we provide an overview of the fundamental properties of point defects and dopants as well as their complexes in bulk crystals and nanostructures. Nominally undoped ZnO is typically n-type, which has been widely ascribed to O vacancies or Zn interstitials; however, these defect assignments are controversial as O vacancies are deep donors while Zn interstitials are highly mobile at room temperature and considered to be unstable. Accordingly, H and group III impurities have also been suggested to be responsible for the observed n-type conductivity. Although there are still many unanswered questions concerning defect-related luminescence bands in ZnO, great progress has been made in recent years to identify and characterize them using spatially resolved luminescence spectroscopies and first-principles calculations. The ubiquitous green emission has several possible origins, including O and Zn vacancies as well as Cu impurities. The properties of group I (Li, Na, and Cu), group III (Ga, Al,

and In), and group V (N, P, and Sb) impurities as well as their complexes with native point defects and H are discussed, along with a concluding outlook for future research into the optical properties of ZnO.

1. Introduction

Zinc oxide is a wide-bandgap semiconductor with great potential for numerous applications such as solid-state lighting [1, 2], solar cells [3], lasing [4], and sensors [5]. With a large exciton binding energy of 60 meV, ZnO emits light efficiently in the UV region of the spectrum, making it a strong candidate for optical devices. In contrast to GaN, large crystals of ZnO can be grown easily and the low cost of Zn makes ZnO economically competitive for large-scale device fabrication. While ZnO have inherent advantages, the lack of control over native defects and impurities presents a major obstacle to the realization of practical devices. The presence of such defects and impurities can inhibit the performance of devices due to detrimental effects such as nonradiative recombination, carrier trapping, as well as parasitic luminescence and absorption. The literature in this area is vast, and only reasonably well-established results are discussed in this chapter. For readers interested in a complete critical discussion on the structural and physical properties of ZnO materials and devices, excellent comprehensive review articles have been published by other workers [6–8].

2. Point Defects in ZnO

2.1. *Intrinsic point defects*

Several theoretical and experimental studies of defect formation in ZnO have been reported [6, 9, 10], and the calculated energy levels of different defects as a function of Fermi level position are displayed in Fig. 1. These data show that defects such as O and Zn vacancies have lowest formation energies in Zn- and O-rich ZnO, respectively. Accordingly, Zn vacancies play a dominant role as compensating acceptors in n-type ZnO. O vacancies are present in significant

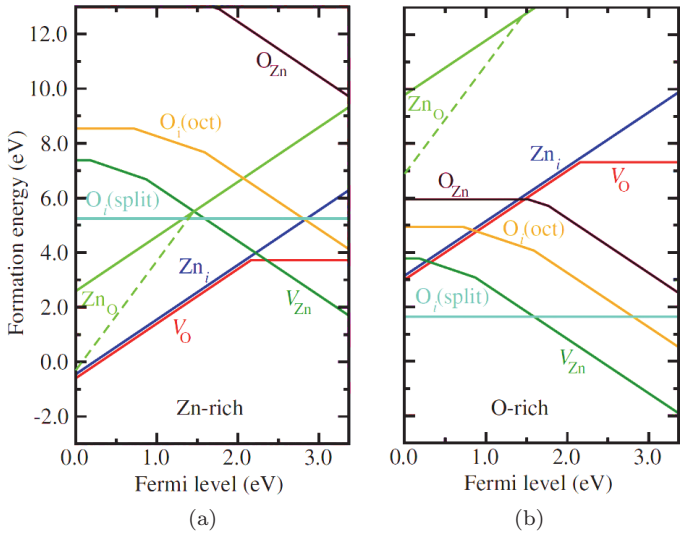

Figure 1. Calculated formation energies of native defects as a function of Fermi level for (a) Zn-rich and (b) O-rich ZnO. The zero of Fermi-level indicates the valence band maximum and the slope corresponding to the charge states. Positive slopes correspond to positively charged defects, indicating their donor-like behavior. Negative slopes indicate negatively charged defects and acceptor-type behavior. Reprinted with permission from [12].

concentration but unlikely to be the dominant cause of n-type conductivity in nominally undoped ZnO due to their deep donor nature, while Zn interstitials are unstable at room temperature due to their high mobility [11, 12]. Other native point defects including oxygen antisites (O_{Zn}) and zinc antisites (Zn_O) are typically not abundant in ZnO under equilibrium conditions due to their high formation energies; the effect of these defects on the properties of (Zn_O) is not discussed further in this chapter. Table 1 provides a summary of the reported energy-level positions of the four main point defects in ZnO: zinc vacancy (V_{Zn}), oxygen vacancy (V_O), zinc interstitial (Zn_i), and oxygen interstitial (O_i).

2.1.1. *Oxygen vacancies*

O vacancies have the lowest formation energy among the native donor-like defects (Fig. 1) and have frequently been cited as the cause

Table 1. Summary of energy positions of native point defects in different charge states in ZnO.

Native defect	Charge state	Energy level (eV)	References
V_{O}	0	$E_c - 0.05$	[25]
	1+	$E_c - 2.0$, $E_c - 1.92$, $E_c - 2.24$	[25–27]
	2+	$E_c - 1.0$, $E_c - 1.1$	[13, 19]
Zn_i	0	$E_c - 0.05$	[25, 26]
	1+	$E_c - 0.5$, $E_c - 0.2$	[25, 26]
	2+	$E_c - 0.15$, $E_c - 0.08$	[14, 28]
V_{Zn}	0	$E_v + 0.3$, $E_v + 0.31$	[29, 30]
	1−	$E_v + 0.7$, $E_v + 0.82$	[25, 26]
	2−	$E_v + 2.8$, $E_v + 2.91$, $E_v + 2.67$	[25, 27]
O_i	0	$E_v + 1.08$, $E_v + 0.9$	[29, 31]
	1−	$E_v + 0.38$, $E_v + 0.4$	[31, 32]
	2−	$E_v + 0.99$, $E_v + 1.43$ $E_v + 0.79$	[30, 32]

of n-type conductivity in ZnO. However, first-principles calculations show that the V_{O} is a deep, negative U donor, where the 1+ charge state is thermodynamically unstable [6, 12, 13], converting spontaneously to either its 2+ or 0 charge state. O vacancies become neutral when the Fermi level is close to the conduction band and above the V_{O} 0/2+ charge transition level. Conversely, when the Fermi level is below the 0/2+ level, V_{O} have a charge of $+2e$ and can act as a source of compensation in p-type ZnO. The position of the 0/2+ charge transition level for O vacancies was calculated to be 1–2 eV below the conduction band maximum [14, 15].

A green luminescence band is commonly observed in both bulk and nanostructured ZnO materials and has been controversially attributed to O vacancies [16–18]. The difficulty in identifying the origin of this defect band is the fact that it is broad and often overlaps with other broad visible emission peaks, which leads to inaccuracy in the measurement of the green emission peak's position, width, and intensity without the use of careful curve fitting. The reported peak energy of V_{O}-related green luminescence varies from 2.42 to 2.54 eV (Table 2). Ye *et al.* [19] reported that the radiative recombination of an electron from the V_{O}^{+} state to the valence band is responsible for the 2.5-eV green emission band, whereas Hofmann *et al.* [20] reported

Table 2. Summary of energy positions and the proposed defects responsible for deep-level emissions in ZnO.

Peak position (eV)	Emission color	Proposed defect	References
2.2–2.5	Green	V_o	[16–18, 20, 43, 47]
2.3–2.5	Green	V_{Zn}	[17, 18, 47]
2.4	Structured green		[48, 49]
2.7–3.1	Blue		[27, 35, 41]
1.7	Red		[50]
2.3	Green	O_i	[47]
2.0–2.1	Yellow/Orange		[43, 44, 51]
1.8–2.0	Red		[35, 41, 45]
2.5–2.7	Blue	Zn_i	[40, 52]
2.85	Violet		[41]

that the optical excitation can convert only a fraction of V_O to V_O^+, which is thermodynamically unstable. It is noted that the different energies of the "green" band in different studies could be associated with different defects; we observed two distinct emission bands at 2.30 and 2.52 eV, attributable to Zn and O vacancies, respectively (see Fig. 2) [18].

2.1.2. *Zinc vacancies*

Zn vacancies in ZnO are double acceptors and have a negligible concentration in p-type ZnO because of their high formation energy. On the contrary, V_{Zn} has the lowest formation energy among native point defects and is present in a moderate concentration in donor-doped ZnO [12]. These acceptors are more favorable to form in the O-rich environment (Fig. 1). Positron annihilation experiments have confirmed that Zn vacancies are dominant compensating acceptors in n-type ZnO [21]. Theoretical and experiments results have been reported for the energy level of V_{Zn} in different charge states (Table 1). In semiconductor terminology, the charge transition level of a defect is defined as the position of Fermi level at which the two charge states of this defect have equal formation energies. First-principles calculations reported the 0/1– and 1–/2– acceptor charge transition levels of V_{Zn} at 0.18–0.2 eV and 0.87–1.2 eV above the

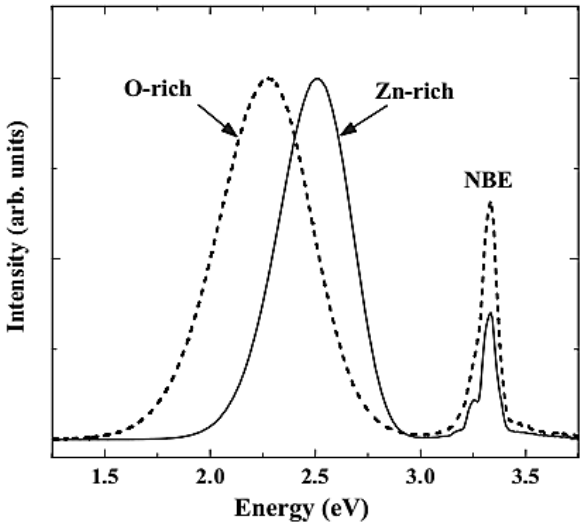

Figure 2. Cathodoluminescence spectra of Zn- and O-rich ZnO particles at 80 K (beam energy = 15 keV, beam current = 0.25 nA) normalized to the green peak height. Both Zn- and O-rich ZnO exhibit near-band-edge emission at 3.35 eV but different green emission peak energies of 2.52 and 2.30 eV, respectively. Reprinted with permission from [18].

valence band maximum, respectively [11, 12], whereas these levels were calculated to be at 0.9 and 1.5 eV, respectively, by generalized gradient approximation (GGA) calculations [22]. When the Fermi level lies above the 1–/2– level, the equilibrium charge state is a negatively charged double acceptor V_{Zn}^{2-}, which is formed by accepting two electrons from the valence band. Electron paramagnetic resonance (EPR) experiments have shown that the 1–/2– level of V_{Zn} lies at $\sim$1.0 eV above the valence band maximum [23, 24]. The slight variation in these data can be attributed to different calculation methods, or in the case of experiment, to diverse sample types, fabrication techniques, and growth conditions.

Zn vacancies are also considered to be responsible for the green emission band in ZnO [17, 18]. Sekiguchi *et al.* provided a strong argument in favor of Zn vacancies being the origin of green emission [33, 34]. The authors reported that the hydrogen plasma treatment strongly passivates the green emission band in ZnO as Zn vacancies

can readily interact with and be passivated by hydrogen. The peak positions of the reported V_{Zn}-related green luminescence are found in the 2.2–2.5 eV energy range (Table 2). Different research groups suggested different types of electronic transitions involving V_{Zn} defects to describe the green emission band, such as a shallow donor to a deep V_{Zn} acceptor [35], from the conduction band to V_{Zn} acceptor [27], from a Zn_i donor to V_{Zn} acceptor level [36], and a hole transfer from divalent zinc vacancy (V_{Zn}^{2-}) and a monovalent (V_{Zn}^{-}) defect [37]. The defect center responsible for the green luminescence in ZnO remains controversial.

2.1.3. *Zinc interstitials*

In the ZnO wurtzite lattice, Zn interstitials (Zn_i) act as donors and can occupy either octahedral or tetrahedral sites. However, Zn_i is more stable at the octahedral site because the tetrahedral site exhibits a higher formation energy [48]. Among the three charge states of zinc interstitials (Zn_i^{o}, Zn_i^{+}, and Zn_i^{2+}), the most stable state is Zn_i^{2+}, which is formed by donating two electrons to the conduction band. Under equilibrium conditions, Zn_i has a high formation energy in n-type ZnO (as shown in Fig. 1) and is likely to be present in a negligible concentration [48]. Accordingly, Zn_i defects cannot be the source of the background n-type conductivity in ZnO even under Zn-rich conditions [48]. Additionally, there is general consensus that Zn_i are unstable at room temperature due to their high mobility. Nevertheless, it has been suggested that Zn_i defects can be a source of n-type conductivity under non-equilibrium conditions or by forming complexes involving N impurities [10]. For example, Hutson *et al.* reported the presence of Zn_i shallow donors with an activation energy of 51 meV in Hall experiments [38] and Look *et al.* observed the presence of Zn_i shallow donors when ZnO samples were irradiated by a high-energy electron beam [39]. The formation energy of Zn_i falls with decreasing Fermi energy, indicating that they act as a compensating defect in p-type ZnO [48].

Zn_i is not considered to be an optically active luminescence center under equilibrium conditions, but this defect has been reported to be a source of blue and violet emissions in ZnO that was produced in

highly non-equilibrium processes such as laser ablation and Zn-rich annealing [40, 41]. Halliburton *et al.* attributed an increased concentration of free carriers in the ZnO crystal annealed in Zn vapor [42] to Zn_i and proposed that the non-equilibrium conditions promote the formation of this defect. The peak positions of the reported Zn_i-related blue/violet luminescence are found in the 2.54–2.85 eV energy range as summarized in Table 2. Zeng *et al.* assigned the violet and blue emissions to the transitions from Zn_i and extended Zn_i states to the valance band, respectively [40].

2.1.4. *Oxygen interstitials*

Oxygen interstitials (O_i) can occupy either the octahedral interstitial site or tetrahedral interstitial site and are deep acceptors. First-principles calculations suggest that the tetrahedral interstitials are unstable, transforming into a split-interstitial configuration, also known as dumbbell configuration [14]. Conversely, O_i in the octahedral interstitial site are more stable and electrically active [49]. The octahedral O_i introduce –/2– and 0/– acceptor charge transition levels at 1.59 and 0.72 eV above the valence band maximum, respectively [6]. The octahedral O_i configuration has high formation energy and its concentration is negligible in ZnO under equilibrium conditions. Janotti *et al.* reported that oxygen interstitials are electrically inactive in *p*-type ZnO and act as a deep acceptor when the Fermi level is greater than 2.8 eV [6].

A broad yellow emission peaking in the energy range of 2.0–2.1 eV has been reported in ZnO (Table 2) [43, 44]. This yellow emission band in ZnO has been attributed to O_i defects [43, 44]. Moreover, several groups reported that the red emission centered at ~ 1.80 eV in ZnO nanostructures is related to O_i defects [35, 45]. Figure 3 shows the deep level emission of the ZnO film that was annealed in Ar gas at 700°C and 900°C and subsequently treated by remote hydrogen plasma. The annealed ZnO films exhibit green (at 2.35 eV) and yellow (at 2.0 eV) emissions, which are both completely passivated by a hydrogen plasma, where the yellow emission is attributed to O_i defects [46]. The hydrogen plasma passivation of the O_i-related yellow emission band in ZnO is consistent with its assignment to O_i.

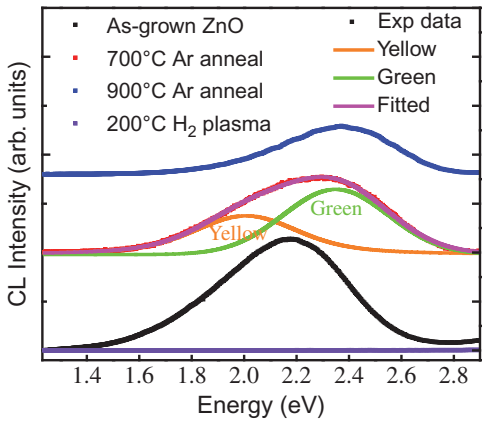

Figure 3. Cathodoluminescence spectra of the as-grown, 700°C and 900°C annealed undoped ZnO films (beam energy = 5 keV, beam current = 3 nA). The modeled CL spectra fitted with the yellow and green luminescence components. The emission spectrum from the film after being treated with remote hydrogen plasma (bottom spectrum) is also included and shows that the plasma treatment completely passivates both the green and yellow emission bands.

In contrast, a similar yellow emission attributed to Li impurities in ZnO is not passivated by an equivalent hydrogen plasma treatment [46].

3. Impurities and Defect Complexes

The control of impurities and their associated charge states is of paramount importance in applications that exploit the wide range of properties of doped ZnO. Intense research efforts have been focused on the fabrication and characterization of acceptor-doped ZnO; however, reports of p-type samples are highly controversial. Incorporation of dopants into ZnO can also change the growth direction of 1D nanostructures; for example, ZnO nanorings and nanobelts can be produced using In as the dopant element [53, 54].

3.1. *Group I elements and hydrogen*

Group I (Li, Na, and K) elements are useful potential dopants for p-type ZnO and have been theoretically predicted to be shallow acceptors when substituting Zn atoms, whereas H (also a group I

element) is a shallow donor. First-principles calculations and experiments have drawn attention to the role of hydrogen on the electronic and optical properties ZnO [55, 56]. It has been reported that that interstitial hydrogen acts as a shallow donor and its positive charge state (H_i^+) is thermodynamically stable [6]. Hydrogen is a common impurity that can be unintentionally incorporated during growth of the most used techniques and can contribute to background n-type conductivity. First-principles calculations showed that hydrogen passivates V_{Zn} by the formation of a thermodynamically stable (V_{Zn}–H_2) neutral complex [34]. These defect complexes are electrically inactive [34]. This result is consistent with the experimental study that H plasma treatment completely passivates the V_{Zn}-related green emission band [18]. More recent theoretical work based on density function calculations suggests that hydrogen can form a H–V_O defect complex with the O vacancy, which has a low formation energy of about 1.7 eV lower than that of H_i [55]. Unlike H_i, this shallow donor complex is considered to be immobile at elevated temperatures and is responsible for the stability of high conductivity in H-doped ZnO films up to 250°C [55].

Group I impurities (Li, Na, and K) at the interstitial sites are donors but act as acceptors at the Zn substitutional site. First-principles calculations have shown that Li, Na, and K elements are found to be deep acceptors located at 0.74, 0.85, and 1.26 meV above the valence band maximum [32, 57]. Based on the optical measurements, Meyer *et al.* and Kushnirenko *et al.* reported that Li_{Zn}, Na_{Zn}, and K_{Zn} are optically active acceptor centers, which give rise to shallow donor to deep acceptor recombination in the visible spectrum [58, 59]. Meyer *et al.* also reported that Li and Na, incorporated either during growth or by diffusion, can introduce acceptors with a hole-binding energy of around 0.3 eV, which shows a donor–acceptor pair recombination [58]. Park *et al.* calculated the ionization energy of 0.09, 0.17, and 0.32 eV for substitutional Li, Na, and K, respectively [60].

A Li-related pair complex (Li_{Zn} + Li_i) can also be formed in ZnO under O-rich conditions [61]. Figures 4(a), 4(b) shows the local

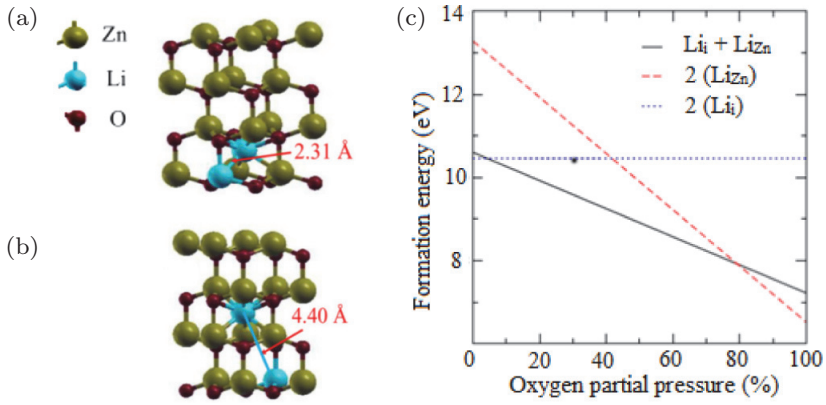

Figure 4. The local atomic geometry of $Li_{Zn} + Li_i$ pair complexes for (a) nearest and (b) well-separated Li species (Reprinted with permission from [62]). (c) Formation energy of the $Li_{Zn} + Li_i$ pair complex as a function of oxygen partial pressure. (Reprinted with permission from [57]).

atomic geometry of the $Li_{Zn} + Li_i$ complex [62]. For both the O-rich and Zn-rich conditions, the formation energy decreases for Li_{Zn} and increases for Li_i with are increase in the Fermi level. Under O-rich conditions, the $Li_{Zn} + Li_i$ pair complex has lower formation energy than either isolated Li_{Zn} or Li_i defect (Fig. 4) [57]. Based on the first-principles calculations and photoluminescence measurements, Sahu *et al.* proposed that this acceptor-like complex is optically active and exhibits a visible emission band at 3.0 eV. EPR experiments showed that Li has two acceptor states at 0.85 and 0.15 eV above the valence band maximum [63].

Group IB elements (Cu, Au, and Ag) act as acceptors when incorporated at Zn sites. Under O-rich conditions, the formation energies of these acceptors are very low, but are considerably higher when located at interstitial sites [64]. The charge transition energies (0/−) for Cu_{Zn}, Ag_{Zn}, and Au_{Zn} are relatively high at 0.7, 0.4, and 0.5 eV above the valence band maximum, respectively [64]. Group IB elements are better p-type dopants than IA elements due to their high ionization energy and less self-compensation by native donor defects. Cu favorably occupies the Zn site, (Cu_{Zn}), which acts as an acceptor leading to the p-type conductivity and ferromagnetism

[65, 66]. Cu is a commonly incorporated impurity up to the ppm level in II–VI semiconductors; a large amount of work on Cu-doped ZnO exists concerning various aspects of Cu acceptor states and their possible role in structured green luminescence in ZnO crystals and nanostructures [67, 68]. Huang *et al.* [69] reported that Cu has three charge states, i.e. Cu^{+}_{Zn} or $Cu^{3+}(3d^{8}4s^{0})$, Cu^{0}_{Zn} or Cu^{2+} $(3d^{9}4s^{0})$, and Cu^{-}_{Zn} or $Cu^{1+}(3d^{10}4s^{0})$. These defects have higher formation energies than native defects of ZnO in Zn-rich conditions and have lower formation energies in O-rich conditions [69]. When the Fermi level is above the Cu^{2+}/Cu^{1+} (0/–) charge transition level, the equilibrium state is Cu^{1+}, which is a negatively charged acceptor. With increasing Cu doping concentration in ZnO, the Cu^{1+} state causes the *p*-type conductivity and the Fermi level shifts toward the valence band until the Cu^{2+}/Cu^{1+} level is reached. First-principles calculations showed that the Cu-doped ZnO is ferromagnetic when Cu atoms are present in ZnO in their Cu^{3+} and Cu^{2+} charge states, which exist only in *p*-type ZnO [69]. Conversely, Cu-doped ZnO was found to be non-magnetic when Cu atoms stay in the Cu^{1+} state. The charge states of Cu can be also mediated by doping ZnO with Ga, which pushes the Fermi level above the Cu^{2+}/Cu^{1+} transition level [68]. The position of this Cu^{2+}/Cu^{1+} level is still a matter of great controversy: Wardle *et al.* [70] estimated this transition level to be at 1.0 eV above the valence band maximum, while Yan *et al.* [64] gave a value of 0.7 eV. Electrical measurements on Cu-doped ZnO revealed that the 0/– level lies at 0.2 eV below the conduction band minimum [71]. Admittance spectroscopy and photoluminescence experiments have shown that Cu has two acceptor levels at $E_c-0.17$ and $E_v+0.4$ eV [72, 73].

3.2. *Group-II element (Mg)*

Mg energetically prefers to occupy the Zn site and induces substitutional defects acting as acceptors in ZnO[74]. Alloying ZnO films with MgO is a commonly used method for tuning the bandgap of ZnO [75]. Mg can also occupy either octahedral interstitial site

(Mg_i^O) or tetrahedral interstitial site (Mg_i^T). The formation energy of Mg_i is higher than that of Mg_{Zn} for all Fermi energies except under Zn-rich conditions where the formation energy of Mg_i is lower when the Fermi level is near the valence band maximum (see Fig. 5) [74]. Since the Fermi level is always close to the conduction band in ZnO due to its inherent n-type conductivity, Mg_{Zn} is the most thermodynamically stable defect type under both O- and Zn-rich conditions. The substitutional Mg_{Zn} in ZnO lowers the formation energy of Zn vacancies (V_{Zn}) by $\sim$2.1 eV and thereby promotes the formation of V_{Zn} centers [76]. This prediction is consistent with the photoluminescence results, revealing that doping ZnO with Mg significantly enhances the V_{Zn}-related green luminescence band [77]. First-principles calculations showed that Mg_{Zn} can interact with the donor-like defects (V_O and Zn_i) of ZnO, forming the $Mg_{Zn} - Zn_i$ and $Mg_{Zn} - V_O$ defect complexes [76]. This is in agreement with the experimental result that Mg doping quenches the V_O-related visible emission band in ZnO [78].

3.3. *Group III elements*

The group III elements (Ga, Al, and In) are well-known n-type dopants in ZnO. Al and Ga are favored donors for transparent conductor applications; high doping levels of $n \sim 10^{20}$ cm^{-3} can make ZnO electrically conductive and optically transparent [79]. Group III elements are preferably incorporated at Zn sites and induce substitutional defects in ZnO [80]. They can also be accommodated at either the octahedral interstitial site (Ga_i^O) or the tetrahedral interstitial site (Ga_i^T). The formation energies of these dopants at interstitial sites are much higher than those on substitutional sites and their concentrations are negligible when grown under equilibrium conditions [80, 81]. Theoretical and experimental studies showed that the group III elements can interact with native acceptor-like defects (V_{Zn} and O_i), generating high concentrations of $Ga_{Zn} - V_{Zn}$ and $Ga_{Zn} - O_i$ defect complexes due to the Coulomb interaction between donor and acceptor centers [82, 83]. The local atomic geometry of $Ga_{Zn} - V_{Zn}$

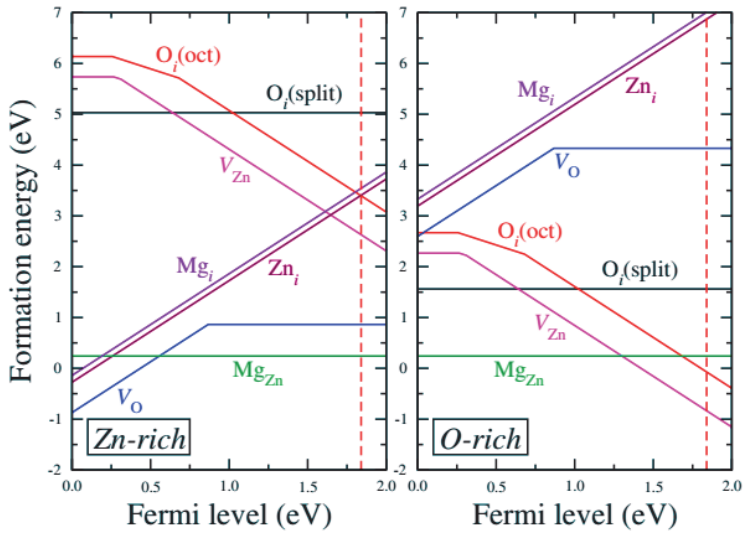

Figure 5. The formation energies of Mg defects in comparison with native defects in ZnO under Zn-rich and O-rich conditions. The Fermi level is referenced to the valence band maximum. Reprinted with permission from [74].

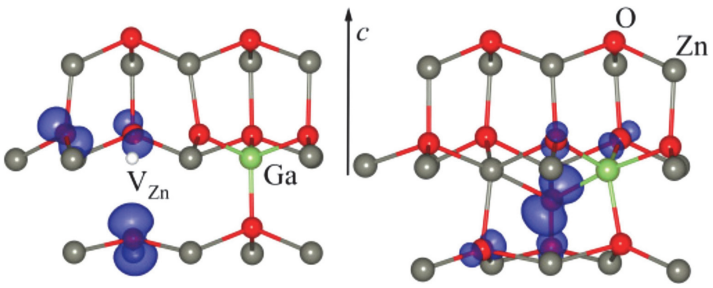

Figure 6. Local atomic geometry for (a) $Ga_{Zn} - V_{Zn}$and (b) $Ga_{Zn} - O_i$ complexes in Ga-doped ZnO. Both defect complexes act as deep acceptors and are electrically active in ZnO. Reprinted with permission from [82].

and $Ga_{Zn} - O_i$ defect complexes are shown in Fig. 6. These defects act as acceptors and are electrically active in ZnO.

Under O-rich conditions, the $Ga_{Zn} - V_{Zn}$ acceptor complex has significantly lower formation energy than the isolated substitutional

Ga_{Zn} donors when the Fermi energy is close to the conduction band minimum (Fig. 6) and is responsible for appreciable defect compensation in highly Ga-doped ZnO. These theoretical predictions were verified by experimental results, which reported that both the electrical conductivity and carrier concentration significantly decrease at high Ga doping concentrations when samples were grown under O-rich conditions [84, 85]. The formation energy of $Ga_{Zn} - O_i$ is higher than $Ga_{Zn} - V_{Zn}$, indicating that the compensation effect due to the $Ga_{Zn} - O_i$ complex in Ga-doped ZnO is weaker. In O-poor conditions, the formation energies of these defect complexes are substantially higher (Fig. 7), suggesting that the compensation mechanism is less pronounced. Several experimental and theoretical studies showed that the $Ga_{Zn} - V_{Zn}$ and $Ga_{Zn} - O_i$ complexes have ionization energies of about 0.75 and 0.66 eV above the valence band maximum, respectively [82, 86].

3.4. *Group IV elements*

Theoretical investigations showed that group IV elements (C, Si, and Sn) act as donors when occupying the Zn site in ZnO and that ZnO can be made highly conductive and transparent in the visible region by doping with Si [87]. However, there has been little evidence that these elements are incorporated at an appreciable level into ZnO crystals. Carbon is a common impurity in chemical vapor transport growth with graphite and MOCVD; it was theoretically predicted that C could either occupy in the substitutional Zn- or O-sites, forming C_{Zn} donor or C_O acceptor [88]. Based on first-principles calculations, Lu *et al.* [89] predicted that C_O interacts with the donor-like defects (V_O and Zn_i), forming $C_O - V_O$, $C_O - Zn_i$, and $2C_O - V_O - Zn_i$ defect complexes. The authors claimed that the $C_O - Zn_i$ and $2C_O - V_O - Zn_i$ complexes have a low formation energy as shown in Fig. 8 and are the possible source of green and red emissions in ZnO, respectively. This prediction is consistent with photoluminescence studies of C-doped ZnO [90]. Combination of density function calculations and optical measurements showed that Sn doping of ZnO quantum dots eliminates V_O while creating O_{Zn} and

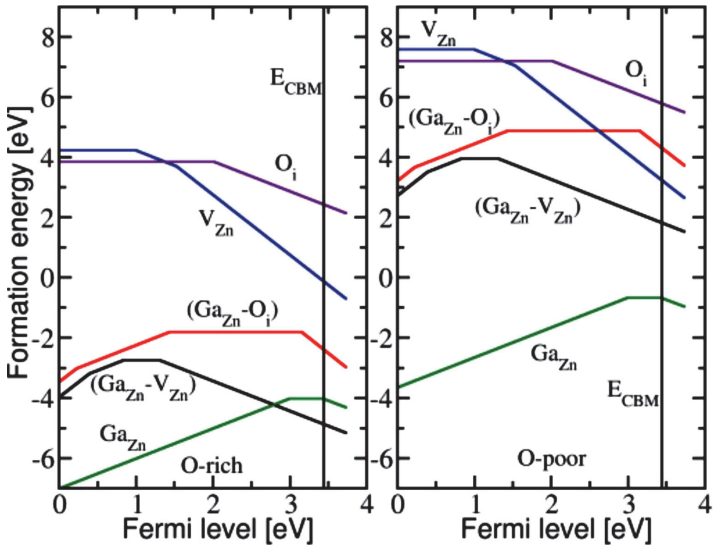

Figure 7. Formation energies of Ga-related defects as a function of Fermi level in (a) O-rich and (b) O-poor conditions. The zero value of the Fermi level corresponds to the valence band maximum and the "kinks" in the curves indicate transitions between the defect charge states. Under the O-rich condition, both $Ga_{Zn} - V_{Zn}$ and $Ga_{Zn} - O_i$ complexes can efficiently form due to their low formation energies and play an important role as compensating defects in Ga-doped ZnO. Reprinted with permission from [82].

O_i defects as a result of conversion from Sn^{4+} to Sn^{2+} state with increasing Sn doping concentration [91].

3.5. *Group V elements*

The greatest challenge in research on ZnO is the achievement of reliable and reproducible p-type doping. Group V (N, P, As, and Sb) elements are the most promising candidates for p-type doping, but unfortunately, most of these dopants form deep acceptors. The substitutional X_O (where X = N, P, As, and Sb) at the O site is a deep acceptor and is unlikely to contribute for the p-type conduction in ZnO, while the substitutional X_{Zn} at the Zn site exhibits donor-like behavior [7, 92]. First-principles calculations show that N substituting an O is a deep acceptor with a hole binding energy of 0.4 eV [60],

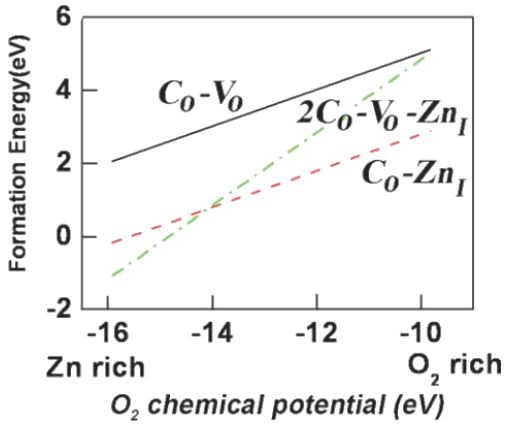

Figure 8. Calculated formation energies of carbon defect complexes as a function of O_2 chemical potential. The complexes are C_O–V_O (black line), C_O–Zn_i(red) and $2C_O$–V_O–Zn_i (green). Reprinted with permission from [89].

while photoluminescence experiments revealed a hole binding energy of ∼0.2 eV [93]. X-ray electron and X-ray absorption spectroscopies on N-doped ZnO showed that N exists in three chemical states, attributed to N_O, N_{Zn}, and N_2 molecules, and a direct correlation was observed between the N-related donor–acceptor pair emission and the concentration of N_2 [94, 95]. The experimental observations are in agreement with first-principles calculations which predict that N_2 at the Zn site is a shallow acceptor [96].

P, As, and Sb have significantly larger ionic radii than O, and according to the first-principles calculations, they act as deep acceptors when accommodated at the O substitutional site [60]. Nevertheless, p-type conductivity in P-doped ZnO has been reported by several groups [97, 98]. Modeling also predicted that the substitutional X_{Zn} interacts with Zn vacancies, forming an acceptor complex $X_{Zn}-2V_{Zn}$ [92, 99]. The formation energies of P-induced defects and complexes in ZnO are displayed in Fig. 8. Under O-rich conditions, the $P_{Zn}-2V_{Zn}$ acceptor complex has a lower formation energy than the other defects, the calculated transition level (+/−) for this complex is 150 meV above the valence band maximum [99]. This calculated value seems to be in qualitative agreement with the experimental investigations that report an acceptor level in the range

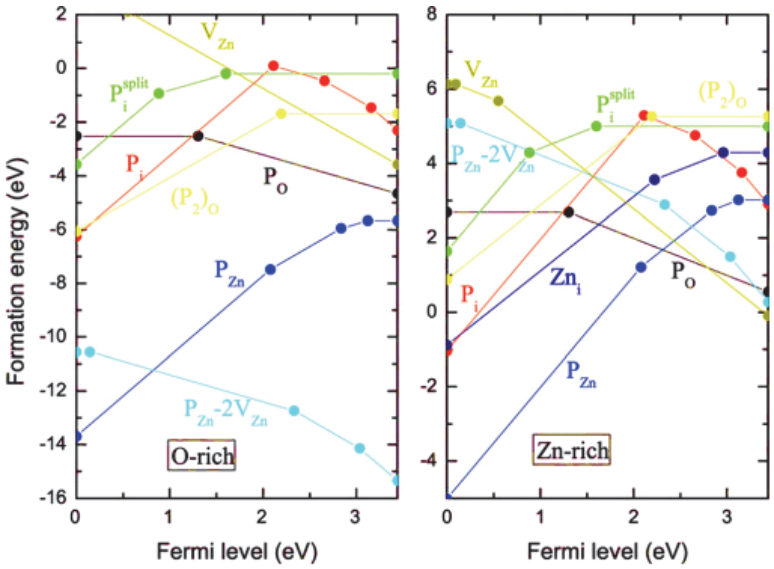

Figure 9. Formation energy of native and P-induced defects in ZnO under O-rich and Zn-rich conditions. Reprinted with permission from [99].

of 120 – 180 meV for P-doped ZnO [98, 100]. Photoluminescence and Hall measurements of Sb-doped ZnO films also showed that the incorporation of Sb induces the formation of $Sb_{Zn}-2V_{Zn}$ shallow acceptor complex with a binding energy 161 meV, responsible for their p-type conduction [101]. Further experiments and modeling need to be performed to confirm the microscopic structure of these acceptor complexes.

4. Conclusions

Recent theoretical and experimental investigations have provided further insight into the nature of point defects, impurities, and dopants in ZnO and their effect on the electrical and optical properties. Significant progress has been made in recent years in fabricating of high-quality ZnO samples suitable for detailed and systematic investigations of defect characteristics. Yet, several significant questions concerning the fundamental properties of defects and their roles in the performance of ZnO-based devices remain largely

unresolved. The ultimate goal of being able to reproducibly fabricate, high-quality p-type ZnO has not been met. This review emphasizes that comprehensive studies aimed at understanding and controlling native and impurity-induced defects are essential for the development of practical ZnO devices with bespoke properties for specific applications. Elements in several periodic table groups have been considered as potential dopants in ZnO. The electronic and optical properties of the host ZnO were found to be influenced in a similar way upon doping with elements from the same group. Group I elements act as deep acceptors when residing on a substitutional Zn site and are responsible for the yellow emission in ZnO. Group I atoms at interstitial sites behave as shallow acceptors and have been reported to yield p-type conductivity in ZnO, but the exact nature of these acceptors is not yet clear. Mg from group II has been proved effective in engineering the bandgap of ZnO. Group III elements, specifically Al, Ga, and H, account for the n-type behavior of ZnO in most circumstances. Al and Ga are the preferred donors for transparent conductor applications, but these donors could be compensated via the formation of acceptor complexes with either Zn vacancies or O interstitials. Both of the acceptor complex types are known to be electrically and optically active. Little is known about the incorporation of C and Si, but many studies claim that these group IV dopants can make ZnO films highly conductive for transparent electrical contacts. Group V dopants, in particular N and P, are considered to be the natural choice for p-type doping; however, the origin of p-type response in ZnO doped with N or P remains controversial due to the formation of compensating defects and their low solubility. ZnO holds great promise for a range of photonic and optoelectronic applications, it is hoped that new fundamental insights from reliable characterization of defects will lead to transformative breakthroughs in practical ZnO devices.

Acknowledgments

Financial support from the Australian Research Council (ARC) under the Discovery Project funding scheme (project number DP150103317) is acknowledged.

References

[1] X. Huang, *Nat. Photon.* **8**, 748 (2014).
[2] M. A. Rahman, J. A. Scott, A. Gentle, M. R. Phillips, C. Ton-That, *Nanotechnology* **29**, 425707 (2018).
[3] Y. Tang, Z. Chen, H. Song, C. Lee, H. Cong, H. Cheng, W. Zhang, I. Bello, S. Lee, *Nano Lett.* **8**, 4191 (2008).
[4] S. Chu, G. Wang, W. Zhou, Y. Lin, L. Chernyak, J. Zhao, J. Kong, L. Li, J. Ren, J. Liu, *Nat. Nanotechnol.* **6**, 506 (2011).
[5] S. N. Das, J. P. Kar, J.-H. Choi, T. I. Lee, K.-J. Moon, J.-M. Myoung, *J. Phys. Chem. C* **114**, 1689 (2010).
[6] A. Janotti and C. G. Van de Walle, Rep. Prog. Phys. **72**, 126501 (2009).
[7] Ü. Özgür, Y. I. Alivov, C. Liu, A. Teke, M. Reshchikov, S. Doğan, V. Avrutin, S.-J. Cho, H. Morkoc, *J. Appl. Phys.* **98**, 11 (2005).
[8] A. B. Djurisic, A. M. C. Ng, X. Y. Chen, *Prog. Quant. Electron.* **34**, 191 (2010).
[9] F. Selim, M. Weber, D. Solodovnikov, K. Lynn, *Phys. Rev. Lett.* **99**, 085502 (2007).
[10] D. C. Look, G. C. Farlow, P. Reunchan, S. Limpijumnong, S. Zhang, K. Nordlund, *Phys. Rev. Lett.* **95**, 225502 (2005).
[11] A. Kohan, G. Ceder, D. Morgan, C. G. Van de Walle, *Phys. Rev. B* **61**, 15019 (2000).
[12] A. Janotti, C. G. Van de Walle, *Phys. Rev. B* **76**, 165202 (2007).
[13] A. Janotti, C. G. Van de Walle, *Appl. Phys. Lett.* **87**, 122102 (2005).
[14] P. Erhart, K. Albe, A. Klein, *Phys. Rev. B* **73**, 205203 (2006).
[15] A. Janotti, C. G. Van de Walle, *Nat. Mater.* **6**, 44 (2007).
[16] F. Leiter, H. Alves, A. Hofstaetter, D. Hofmann, B. Meyer, *Phys. Status Solidi B* **226**, R4 (2001).
[17] T. M. Børseth, B. Svensson, A. Y. Kuznetsov, P. Klason, Q. Zhao, M. Willander, *Appl. Phys. Lett.* **89**, 262112 (2006).
[18] C. Ton-That, L. Weston, M. Phillips, *Phys. Rev. B* **86**, 115205 (2012).
[19] J. Ye, S. Gu, F. Qin, S. Zhu, S. Liu, X. Zhou, W. Liu, L. Hu, R. Zhang, Y. Shi, *Appl. Phys. A* **81**, 759 (2005).
[20] D. Hofmann, D. Pfisterer, J. Sann, B. Meyer, R. Tena-Zaera, V. Munoz-Sanjose, T. Frank, G. Pensl, *Appl. Phys. A* **88**, 147 (2007).
[21] F. Tuomisto, V. Ranki, K. Saarinen, D. C. Look, *Phys. Rev. Lett.* **91**, 205502 (2003).
[22] S. Lany, A. Zunger, *Phys. Rev. Lett.* **98**, 045501 (2007).
[23] X. Wang, L. Vlasenko, S. Pearton, W. Chen, I. A. Buyanova, *J. Phys. D: Appl. Phys.* **42**, 175411 (2009).
[24] S. Evans, N. Giles, L. Halliburton, L. Kappers, *J. Appl. Phys.* **103**, 043710 (2008).
[25] S. Lima, F. Sigoli, M. Jafelicci Jr, M. R. Davolos, *Int. J. Inorg. Mater.* **3**, 749 (2001).

[26] V. Nikitenko, *Zinc Oxide — A Material for Micro-and Optoelectronic Applications* (Springer, 2005), p. 69.
[27] P. Thiyagarajan, M. Kottaisamy, N. Rama, M. R. Rao, *Scripta Mater.* **59**, 722 (2008).
[28] A. Djurišić, A. Ng, X. Chen, *Prog. Quant. Electron.* **34**, 191 (2010).
[29] B. Lin, Z. Fu, Y. Jia, *Appl. Phys. Lett.* **79**, 943 (2001).
[30] S. Choi, M. R. Phillips, I. Aharonovich, S. Pornsuwan, B. C. Cowie, C. Ton-That, *Adv. Opt. Mater.* **3**, 821 (2015).
[31] P. Xu, Y. Sun, C. Shi, F. Xu, H. Pan, *Nucl. Instr. Meth. Phys. Res. B* **199**, 286 (2003).
[32] J. Hu, B. Pan, *J. Chem. Phys.* **129**, 154706 (2008).
[33] C. G. Van de Walle, *Phys. Rev. Lett.* **85**, 1012 (2000).
[34] E. Lavrov, J. Weber, F. Börrnert, C. G. Van de Walle, R. Helbig, *Phys. Rev. B* **66**, 165205 (2002).
[35] N. Alvi, K. Ul Hasan, O. Nur, M. Willander, *Nanoscale Res. Lett.* **6**, 130 (2011).
[36] A. Escobedo-Morales, U. Pal, *Appl. Phys. Lett.* **93**, 193120 (2008).
[37] C. Xu, X. Sun, X. Zhang, L. Ke, S. Chua, *Nanotechnol.* **15**, 856 (2004).
[38] D. Thomas, *J. Phys. Chem. Solids* **3**, 229 (1957).
[39] D. C. Look, J. W. Hemsky, J. Sizelove, *Phys. Rev. Lett.* **82**, 2552 (1999).
[40] H. Zeng, G. Duan, Y. Li, S. Yang, X. Xu, W. Cai, *Adv. Funct. Mater.* **20**, 561 (2010).
[41] C. H. Ahn, Y. Y. Kim, D. C. Kim, S. K. Mohanta, H. K. Cho, *J. Appl. Phys.* **105**, 013502 (2009).
[42] L. Halliburton, N. Giles, N. Garces, M. Luo, C. Xu, L. Bai, L. A. Boatner, *Appl. Phys. Lett.* **87**, 172108 (2005).
[43] X. Wu, G. Siu, C. Fu, H. Ong, *Appl. Phys. Lett.* **78**, 2285 (2001).
[44] A. R. Gheisi, C. Neygandhi, A. K. Sternig, E. Carrasco, H. Marbach, D. Thomele, O. Diwald, *Phys. Chem. Chem. Phys.* **16**, 23922 (2014).
[45] X. Liu, X. Wu, H. Cao, R. Chang, *J. Appl. Phys.* **95**, 3141 (2004).
[46] Z. Wang, C. Luo, W. Anwand, A. Wagner, M. Butterling, M. A. Rahman, M. R. Phillips, C. Ton-That, M. Younas, S. Su, *Sci. Rep.* **9**, 3534 (2019).
[47] J. Lv, C. Li, *Appl. Phys. Lett.* **103**, 232114 (2013).
[48] D. Reynolds, D. C. Look, B. Jogai, *J. Appl. Phys.* **89**, 6189 (2001).
[49] S. Anantachaisilp, S. M. Smith, C. Ton-That, S. Pornsuwan, A. R. Moon, C. Nenstiel, A. Hoffmann, M. R. Phillips, *J. Lumin.* **168**, 20 (2015).
[50] S. Anantachaisilp, S. M. Smith, C. Ton-That, T. Osotchan, A. R. Moon, M. R. Phillips, *J. Phys. Chem. C* **118**, 27150 (2014).
[51] V. Kumar, H. Swart, O. Ntwaeaborwa, R. Kroon, J. Terblans, S. Shaat, A. Yousif, M. Duvenhage, *Mater. Lett.* **101**, 57 (2013).
[52] M. Patra, K. Manzoor, M. Manoth, S. Vadera, N. Kumar, *J. Lumin.* **128**, 267 (2008).
[53] X. Y. Kong, Y. Ding, R. Yang, Z. L. Wang, *Science* **303**, 1348 (2004).
[54] X. Y. Kong, Z. L. Wang, *Nano Lett.* **3**, 1625 (2003).

[55] W. Chen, L. Zhu, Y. Li, L. Hu, Y. Guo, H. Xu, Z. Ye, *Phys. Chem. Chem. Phys.* **15**, 17763 (2013).
[56] R. C. Wang, C. F. Cheng, *Plasma Process. Polym.* **12**, 51 (2015).
[57] R. Vidya, P. Ravindran, H. Fjellvåg, *J. Appl. Phys.* **111**, 123713 (2012).
[58] B. K. Meyer, J. Stehr, A. Hofstaetter, N. Volbers, A. Zeuner, J. Sann, *Appl. Phys. A* **88**, 119 (2007).
[59] V. Kushnirenko, I. Markevich, T. Zashivailo, *J. Lumin.* **132**, 1953 (2012).
[60] C. Park, S. Zhang, S.-H. Wei, *Phys. Rev. B* **66**, 073202 (2002).
[61] A. Carvalho, A. Alkauskas, A. Pasquarello, A. Tagantsev, N. Setter, *Phys. Rev. B* **80**, 195205 (2009).
[62] R. Sahu, K. Dileep, B. Loukya, R. Datta, *Appl. Phys. Lett.* **104**, 051908 (2014).
[63] C. Rauch, W. Gehlhoff, M. Wagner, E. Malguth, G. Callsen, R. Kirste, B. Salameh, A. Hoffmann, S. Polarz, Y. Aksu, *J. Appl. Phys.* **107**, 024311 (2010).
[64] Y. Yan, M. Al-Jassim, S.-H. Wei, *Appl. Phys. Lett.* **89**, 181912 (2006).
[65] D. Buchholz, R. Chang, J.-Y. Song, J. Ketterson, *Appl. Phys. Lett.* **87**, 082504 (2005).
[66] C.-L. Hsu, Y.-D. Gao, Y.-S. Chen, T.-J. Hsueh, *ACS Appl. Mater. Interfaces* **6**, 4277 (2014).
[67] N. Garces, L. Wang, L. Bai, N. Giles, L. Halliburton, G. Cantwell, *Appl. Phys. Lett.* **81**, 622 (2002).
[68] M. A. Rahman, M. T. Westerhausen, C. Nenstiel, S. Choi, A. Hoffmann, A. Gentle, M. R. Phillips, C. Ton-That, *Appl. Phys. Lett.* **110**, 121907 (2017).
[69] D. Huang, Y.-J. Zhao, D.-H. Chen, Y.-Z. Shao, *Appl. Phys. Lett.* **92**, 182509 (2008).
[70] M. Wardle, J. Goss, P. Briddon, *Phys. Rev. B* **72**, 155108 (2005).
[71] E. Mollwo, G. Müller, P. Wagner, *Solid State Commun.* **13**, 1283 (1973).
[72] M. A. Reshchikov, V. Avrutin, N. Izyumskaya, R. Shimada, H. Morkoc, S. Novak, *J. Vac. Sci. Technol.* **27**, 1749 (2009).
[73] Y. Kanai, *Jpn. J. Appl. Phys.* **30**, 703 (1991).
[74] N. Palakawong, J. Jutimoosik, J. T-Thienprasert, S. Rujirawat, S. Limpijumnong, *Integrated Ferroelectrics* **156**, 72 (2014).
[75] A. K. Sharma, J. Narayan, J. F. Muth, C. W. Teng, C. Jin, A. Kvit, R. M. Kolbas, O. W. Holland, *Appl. Phys. Lett.* **75**, 3327 (1999).
[76] R. Dutta, N. Mandal, *Appl. Phys. Lett.* **101**, 042106 (2012).
[77] E. B. Manaia, R. C. K. Kaminski, B. L. Caetano, V. Briois, L. A. Chiavacci, C. Bourgaux, *Eur. J. Nanomed.* **7**, 109 (2015).
[78] J. Perkins, G. Foster, M. Myer, S. Mehra, J. Chauveau, A. Hierro, A. Redondo-Cubero, W. Windl, L. Brillson, *APL Mater.* **3**, 062801 (2015).
[79] H. J. Ko, Y. F. Chen, S. K. Hong, H. Wenisch, T. Yao, D. C. Look, *Appl. Phys. Lett.* **77**, 3761 (2000).
[80] R. Saniz, Y. Xu, M. Matsubara, M. Amini, H. Dixit, D. Lamoen, B. Partoens, *J. Phys. Chem. Solids* **74**, 45 (2013).

[81] Y.-S. Lee, Y.-C. Peng, J.-H. Lu, Y.-R. Zhu, H.-C. Wu, *Thin Solid Films* **570**, 464 (2014).
[82] D. Demchenko, B. Earles, H. Liu, V. Avrutin, N. Izyumskaya, Ü. Özgür, H. Morkoç, *Phys. Rev. B* **84**, 075201 (2011).
[83] M.-H. Lee, Y.-C. Peng, H.-C. Wu, *J. Alloys Compd.* **616**, 122 (2014).
[84] T. Yamada, K. Ikeda, S. Kishimoto, H. Makino, T. Yamamoto, *Surf. Coat. Technol.* **201**, 4004 (2006).
[85] C.-Y. Tsay, K.-S. Fan, C.-M. Lei, *J. Alloys Compd.* **512**, 216 (2012).
[86] A. Tang, Z. Mei, Y. Hou, L. Liu, V. Venkatachalapathy, A. Azarov, A. Kuznetsov, X. Du, *Sci. China Phys., Mech. & Astron.* **61**, 077311 (2018).
[87] J. Liu, X. Fan, C. Sun, W. Zhu, *Chem. Phys. Lett.* **649**, 78 (2016).
[88] S. Panpan, S. Xiyu, H. Qinying, L. Yadong, C. Wei, *J. Semicond.* **30**, 052001 (2009).
[89] Y. Lu, Z. Hong, Y. Feng, S. Russo, *Appl. Phys. Lett.* **96**, 091914 (2010).
[90] L. Tseng, J. Yi, X. Zhang, G. Xing, H. Fan, T. Herng, X. Luo, M. Ionescu, J. Ding, S. Li, *AIP Adv.* **4**, 067117 (2014).
[91] W. Yang, B. Zhang, Q. Zhang, L. Wang, B. Song, Y. Ding, C. Wong, *RSC Adv.* **7**, 11345 (2017).
[92] G. Petretto, F. Bruneval, *Phys. Rev. Appl.* **1**, 024005 (2014).
[93] B. Meyer, Alves, H, D. Hofmann, W. Kriegseis, D. Forster, F. Bertram, J. Christen, A. Hoffmann, M. Straßburg, M. Dworzak, *Phys. Status Solidi B* **241**, 231 (2004).
[94] C. Ton-That, L. Zhu, M. N. Lockrey, M. R. Phillips, B. C. C. Cowie, A. Tadich, L. Thomsen, S. Khachadorian, S. Schlichting, N. Jankowski, A. Hoffmann, *Phys. Rev. B* **92**, 7 (2015).
[95] C. L. Perkins, S. H. Lee, X. N. Li, S. E. Asher, T. J. Coutts, *J. Appl. Phys.* **97**, 7 (2005).
[96] W. R. L. Lambrecht, A. Boonchun, *Phys. Rev. B* **87**, 195207 (2013).
[97] K. K. Kim, H. S. Kim, D. K. Hwang, J. H. Lim, S. J. Park, *Appl. Phys. Lett.* **83**, 63 (2003).
[98] A. Allenic, W. Guo, Y. Chen, M. B. Katz, G. Zhao, Y. Che, Z. Hu, B. Liu, S. B. Zhang, X. Pan, *Adv. Mater.* **19**, 3333 (2007).
[99] P. Li, S.-H. Deng, J. Huang, *Appl. Phys. Lett.* **99**, 111902 (2011).
[100] A. Allenic, W. Guo, Y. Chen, Y. Che, Z. Hu, B. Liu, X. Pan, *J. Phys. D: Appl. Phys.* **41**, 025103 (2007).
[101] X. Pan, W. Guo, Z. Ye, B. Liu, Y. Che, H. He, X. Pan, *J. Appl. Phys.* **105**, 113516 (2009).